Atomistic simulations reveal shape memory of fcc metal nanowires

Wuwei Liang and Min Zhou*

School of Materials Science and Engineering, George W. Woodruff School of Mechanical Engineering, Georgia Institute of Technology, Atlanta, Georgia 30332-0405, USA

(Received 20 January 2006; published 13 March 2006)

We have previously reported the discovery of a shape memory effect (SME) in single-crystalline fcc Cu nanowires [Nano Lett. **5**, 2039 (2005); J. Eng. Mater. Technol. **127**, 423 (2005)]. This paper reports that the same SME also exists in single-crystalline fcc Ni and Au nanowires with lateral dimensions below 5 nm. Under tensile loading and unloading, these Cu, Ni, and Au nanowires can recover elongations of up to 50%, well beyond the recoverable strains of 5–8% typical for most bulk shape memory alloys. Results of atomistic simulations and evidences from experiments show that this phenomenon only exists at the nanometer scale and is associated with a reversible crystallographic lattice reorientation driven by the high surface-stress-induced internal stresses at the nanoscale. This understanding also explains why these metals do not show an SME at macroscopic scales. The analysis also focuses on the role of twinnability in affecting this phenomenon. It is found that fcc metals with higher tendency for twinning (such as Cu, Au, Ni) show this behavior and fcc metals with low likelihood of twinning (such as Al) do not show this behavior.

I. INTRODUCTION

Shape memory materials have important applications involving coupling, sensing, and actuation because of their ability to recover certain configurations under proper thermomechanical conditions. They are sometimes referred to as "smart materials" because they can function simultaneously as sensors and actuators.[1,2] Until recently, the shape memory effect (SME) and its underlying pseudoelasticity were considered unique to shape memory alloys (SMAs), liquid crystal elastomers, and piezoelectric ceramics.[2] More recent research has shown that pseudoelasticity may also be found at the nanoscale, in gold nanowires[3] and carbon nanotubes.[4,5] Here, we report the discovery of a SME in a class of fcc single-crystalline metal nanowires (including Cu, Ni, and Au) with lateral sizes smaller than approximately 5 nm. This behavior arises from a reversible lattice reorientation within the face-centered-cubic (fcc) crystalline structure and is driven by the surface stress and high surface-to-volume ratios of the one-dimensional nanomaterials,[6] a unique and hitherto unknown mechanism which is different from that for SMAs. This SME exists over a wide range of temperature and is associated with response times on the order of nanoseconds, making the nanowires attractive functional components for a new generation of biosensors, transducers, and interconnects in nanoelectromechanical systems (NEMS).[7,8]

This paper focuses on the deformation mechanism, driving force, and critical temperature for this SME, with a particular emphasis on the role of generalized stacking fault energies in determining the existence of the pseudoelastic behavior. Specifically, an explanation as to why this behavior is observed in some fcc metals (e.g., Cu, Au, Ni) but not in others (such as Al) is given. It is observed that fcc metals showing this effect share the common attribute of having high twinnability, a parameter identified by Tadmor and Hai for quantifying the tendency to form twins in fcc metals (discussed later).[9] For the metals that exhibit this behavior, the levels of recoverable strain and the critical temperature associated with the SME are quantified. Finally, the effect of wire size is discussed and the reason why this phenomenon exists only in nanowires but not in bulk single crystals of the same fcc metals is pointed out.

II. MATERIALS

Single-crystalline nanowires of fcc Cu, Ni, Al, and Au are analyzed. In their free-standing unstressed state, these wires have single-crystalline fcc structures with a ⟨110⟩ axis and {111} transverse surfaces (hereafter denoted as the ⟨110⟩/{111} wire or configuration), as shown in Figs. 1(a) and 1(b). They are fabricated experimentally through a "top-down" approach.[10–20] The fabrication process entails "slicing" square columns of atoms from single-crystalline bulk along the [001], [010], and [100] directions using ion beams and allowing them to undergo relaxation. Driven by surface stresses, the nanocolumns spontaneously transform into the ⟨110⟩/{111} configuration through a lattice reorientation pro-
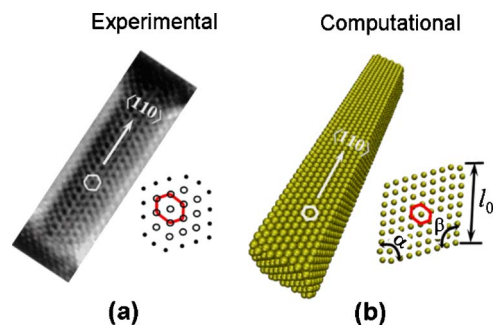
FIG. 1. (Color online) (a) A ⟨110⟩/{111} Au wire cut from a ⟨001⟩/{001} Au nanofilm by electron beam irradiation (reproduced from Ref. 12), (b) a ⟨110⟩/{111} Au wire with rhombic cross sections ($\alpha = 70.5°$ and $\beta = 109.5°$) as predicted by atomistic calculations as the result of the same top-down fabrication process in (a).

TABLE I. Comparison of stacking fault energies.

	γ_{sf} (mJ m^{-2})		γ_{us} (mJ m^{-2})	γ_{ut} (mJ m^{-2})	γ_{sf}/γ_{us}	Twinnability τ_α	Behavior
	EAM	Experiments	EAM	EAM	EAM	EAM	EAM
Cu	45	45[a]	180	202	0.249	0.896	1.040	PE[f] and SME
Ni	125	125[b]	402	460	0.317	0.878	1.020	PE
Au	31	32[c]	101	122	0.307	0.828	0.991	Transitional
Al	146	120–166[d,e]	189	240	0.836	0.788	0.896	Irreversible

[a]Reference 29.
[b]Reference 30.
[c]Reference 31.
[d]Reference 32.
[e]References 33 and 34.
[f]PE=pseudoelasticity.

cess, exhibiting a contraction in the axial direction and an expansion in the lateral directions, as shown in Fig. 1(b). In this paper, the wires with the $\langle 110 \rangle / \{111\}$ configuration are equilibrated at constant temperatures through molecular dynamics (MD) calculations to allow them to assume free-standing states before any mechanical loading. The side length l_0 of the rhombic cross-sections is used to identify the lateral size of the wires. All discussions on size concern this dimension, not the wire length which is sufficiently long so as to not affect the behavior analyzed.

To analyze the wires' mechanical behavior, uniaxial tensile loading and unloading are carried out under simulated quasistatic conditions.[21] Specifically, in each load step, all the atoms are first displaced according to a prescribed uniform strain increment of 0.125% in the length direction. The wires are then equilibrated with their ends fixed at constant temperature for 15 picoseconds (ps) to obtain a macroscopic equilibrium configuration at the prescribed strain. This relaxation process allows structural changes to occur, if the conditions so dictate. This process usually takes less than 12 ps and the average stress over the last 3 ps of the relaxation period at each load step is taken as the stress in the wire at the current strain. Unloading is implemented in the same manner, with a negative strain increment of −0.125%.

Embedded-atom-method (EAM) interatomic potentials are used in the MD simulations. The potentials for Cu, Ni, and Al are developed by Minshin *et al.*[22,23] and the potential for Au is developed by Foiles.[24] In choosing the EAM potentials, special attention is placed on the generalized stacking fault energy (GSFE) including the stable stacking fault energy (SSFE or γ_{sf}), the unstable stacking fault energy (USFE or γ_{us}), and the unstable twinning energy (USTE or γ_{ut}) because of their importance in the nucleation of dislocations and microtwins.[25,26] Rice has shown that γ_{us} is an important parameter in the characterization of dislocation emission.[27] Swygenhoven *et al.* and Tadmor and Hai have demonstrated that the ratios of γ_{sf}/γ_{us} and γ_{us}/γ_{ut} are critical in determining whether deformation occurs via slip or twinning.[9,26] Here, we will demonstrate that the GSFE plays a fundamental role in the pseudoelasticity of fcc nanowires. Since some older EAM potentials have been known to pro-

vide relatively poor approximations of the SSFE of fcc metals, it is important to point out at the outset of this paper that the γ_{sf} predicted by the EAM potentials used in our current analysis are in excellent agreement with experimental measurements or the results of first-principle calculations, as shown in Table I and Fig. 2. We note that while γ_{sf} can be experimentally measured, there are no currently available experimental methods to measure γ_{us} and γ_{ut} directly. Therefore γ_{us} is usually obtained from GSFE curves through first-principle calculations. Since GSFE curves represent the continuous energy cost of rigidly shifting two semi-infinite blocks of crystals on a (111) plane in the $[11\bar{2}]$ direction,[25,26] γ_{us} is defined as the maximum value on the GSFE curve. On the other hand, γ_{sf} is taken as the local minimum between the two γ_{us} peaks. Similarly, γ_{ut} characterizes the energy barrier for creating a microtwin, or a defect in the form of a new extrinsic stacking fault by shifting a layer adjacent to an existing intrinsic stacking fault. The energy variation associated with this process is shown by the dotted lines in Fig. 2 and γ_{ut} is the maximum value on the dotted curve.[9,28] Figure 2 compares the GSFE curves calculated using the EAM potentials with those calculated using the density functional theory (DFT). Obviously, the GSFE curves predicted by the EAM potentials are in good agreement with the results of DFT calculations. The comparison for Au is incomplete because no DFT results are available.

III. MECHANICAL BEHAVIOR

Upon tensile loading and unloading, the nanowires exhibit three types of behavior depending on the material. Specifically,

(1) above a critical temperature T_{cr} (discussed later), Cu and Ni wires exhibit a pseudoelastic behavior with spontaneously reversible strains up to 51%, well beyond the 5%–8% reversible strains typical for most bulk SMAs. Below T_{cr}, the deformation is not spontaneously recoverable and the wires retain their deformed configurations after unloading. For Cu wires, subsequent heating to a temperature above T_{cr} activates the SME and allows the wires to return to their original configurations. For Ni wires, the wires returns
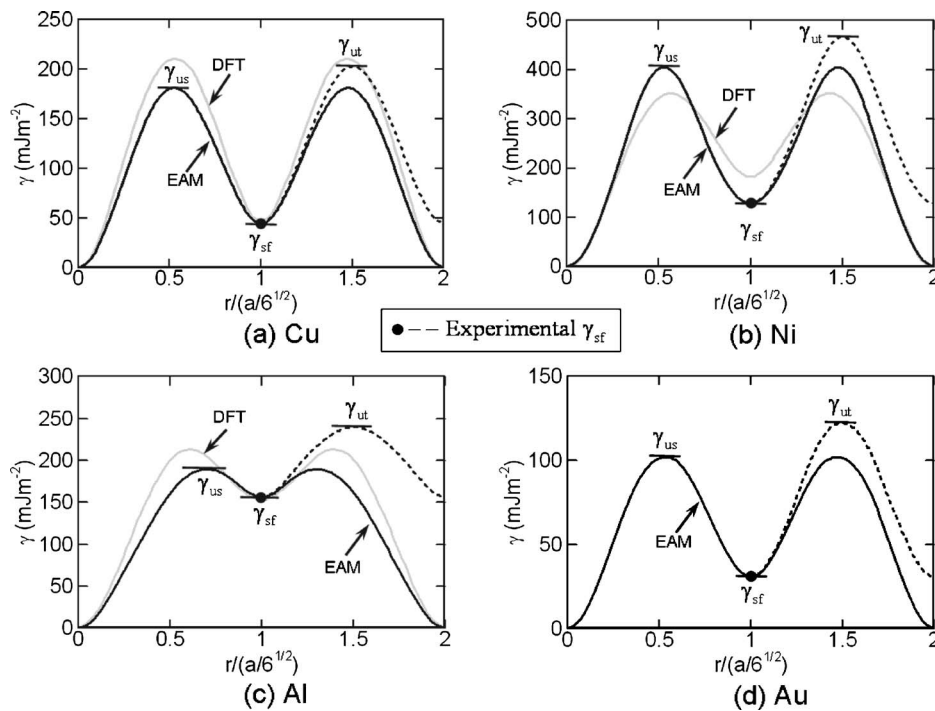
FIG. 2. Generalized planar fault energy curves of Cu, Ni, Al, and Au. The DFT data is from Ref. 25.

to their original configurations only when an external compressive stress is applied;

(2) in contrast, the tensile deformation of Al nanowires is irreversible upon unloading, regardless of temperature; and

(3) Au wires exhibit transitional behaviors from pseudoelasticity like that of Cu and Ni wires at low temperatures to irreversible deformation like that of Al wires at high temperatures.

The different behaviors reported here are associated with, respectively, twinning and slip which are two different but related deformation mechanisms in fcc metals.

A. Pseudoelasticity of Cu and Ni wires

The stress-strain curves in Figs. 3 and 4 show the pseudoelastic behavior upon loading, unloading, and cyclic loading/unloading of Cu and Ni wires which have the $\langle 110 \rangle / \{111\}$ initial configuration. Clearly, the responses are drastically different from those of the corresponding bulk metals. Specifically, the nanowires seem highly ductile with fracture strains of approximately 58%. In comparison, the fracture strains of most bulk fcc metals are usually less than 10%. In Fig. 3(a), the loading path of the stress-strain curves consists of two linear deformation stages (O→A and C→D) followed by two yield points (A and D, respectively), a stage of slow strain hardening over a wide range of strain (B→C), and a stage of precipitous stress drop (D→E). This behavior arises from a unique underlining deformation process. Between O and A, the $\langle 110 \rangle / \{111\}$ wire undergoes elastic stretching. Point A corresponds to the beginning of a lattice reorientation process which leads to a new configuration with a $\langle 001 \rangle$ axis and $\{001\}$ side surfaces (hereafter denoted as the $\langle 001 \rangle / \{001\}$ wire or configuration), as shown in Fig. 5. Between C and D, the newly formed $\langle 001 \rangle / \{001\}$
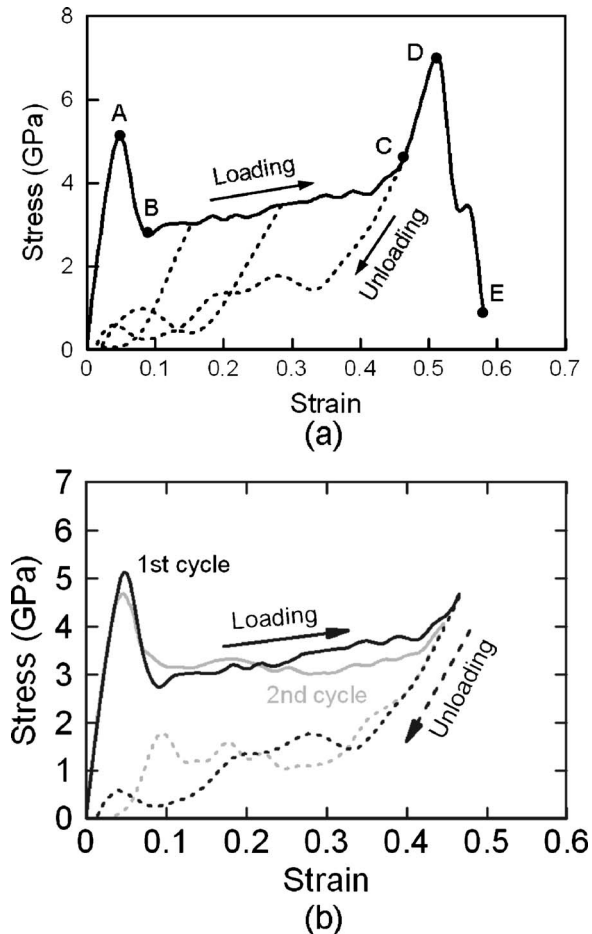
FIG. 3. (a) The stress-strain curves of a 1.8×1.8 nm Cu wire at 200 K during loading and unloading. (b) The same wire under cyclic loading and unloading.
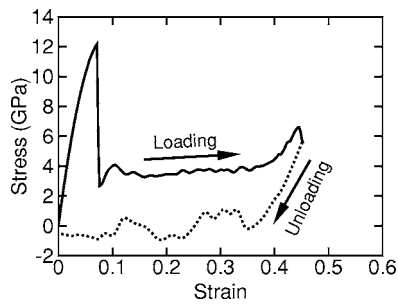
FIG. 4. The stress-strain curve of 2.1×2.1 nm Ni nanowire during loading and unloading at 300 K.

wire undergoes elastic stretching. Further loading beyond D causes the wire to yield through the formation and propagation of full dislocations which ultimately lead to necking and fracture of the nanowire at E.[35]

The unique lattice reorientation process [A→C in Fig. 3(a)] is the key to the pseudoelastic behavior and SME of the wires. The reorientation is completed through the propagation of a {111} twin boundary, which involves repetitive nucleation, gliding, and annihilation of $\frac{1}{6}\langle 112 \rangle$ Shockley partial dislocations, as shown in Fig. 5. Specifically, the partial dislocation is nucleated from one edge, glides across the wire on the {111} plane adjacent to the twin plane, and finally annihilates at the other edge. This process repeats itself and at each cycle the twin boundary propagates by an interplanar distance between two neighboring {111} planes. As the twin boundary sweeps through its length [Fig. 5(a)], the wire is progressively transformed into the new $\langle 001 \rangle$ orientation. Upon the arrival of the twin boundary at the top end of the wire [corresponding to point C in Fig. 3(a)], the whole wire is in the $\langle 001 \rangle /\{100\}$ state. This lattice reorientation process

has been directly observed in experiments during the stretching of Au nanowires.[15] A detailed look at the {111} twin boundary reveals that it has a $[\bar{1}1\bar{2}]$ misorientation axis and a 109.5° misorientation angle (γ) between the lattices on both sides, as shown in Fig. 5(b). The boundary is essentially a $\Sigma 3$ coherent grain boundary separating two nanoscale grains with $\langle 001 \rangle$ and $\langle 110 \rangle$ orientations, respectively. The lattice reorientation essentially progresses through the migration of such $\Sigma 3$ boundaries. This deformation mechanism has been confirmed experimentally in nanocrystalline Cu with grain sizes between 10 and 20 nm.[36]

Upon unloading at temperatures above T_{cr}, the $\langle 001 \rangle /\{001\}$ wire spontaneously transforms back to the original $\langle 110 \rangle /\{111\}$ configuration via a lattice reorientation process in reverse to what is described above for loading. The reversibility of the lattice reorientation from $\langle 110 \rangle /\{111\}$ to $\langle 001 \rangle /\{001\}$ allows the associated deformation to be fully recovered, giving rise to a pseudoelastic behavior of the wire. This reorientation process is driven by the high surface-stress-induced internal stresses in the nanowires and has been observed in experiments and computations for Au nanowires and nanofilms.[12,14,19,37–39] Specifically, spontaneous lattice reorientation from $\langle 001 \rangle$ to $\langle 110 \rangle$ is observed in Au wires when they are cut from Au nanofilms and their free standing configuration is the $\langle 110 \rangle /\{111\}$ structure in Fig. 1(a).[12,40] Furthermore, the same result is also obtained in computations when different atomistic potentials [including an EAM, a modified embedded atom method (MEAM), and a surface embedded atom potential (SEAM)] are used.[14] The spontaneous reverse lattice reorientation allows the tensile deformation to be fully recovered without residual defects. The dashed lines in Figs. 3 and 4 represent the unloading paths from different strains. The loading and unloading paths to-

(a)   (b)
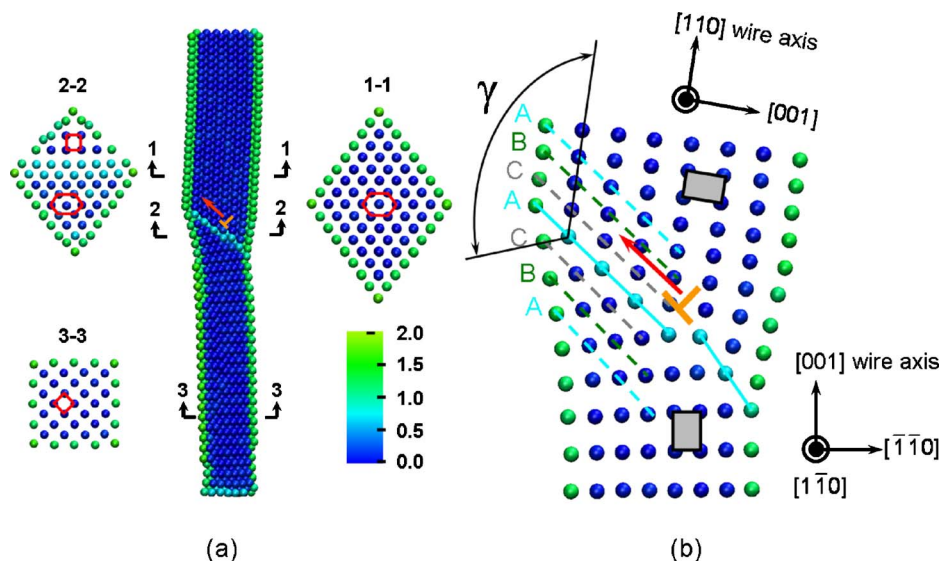
FIG. 5. (Color online) (a) Lattice orientations on the cross sections of a 1.8×1.8 nm Cu nanowire at a strain of 0.24, the middle image shows a sectional view along the wire axis and the $[\bar{1}\bar{1}0]$ diagonal of the cross section, cross-section 1-1 shows the elongated hexagonal lattice in the unrotated domain with the $\langle 110 \rangle /\{111\}$ configuration, cross-section 2-2 is in the transition region containing both the $\langle 001 \rangle /\{001\}$ and the $\langle 110 \rangle /\{111\}$ configurations, and cross-section 3-3 shows the square lattice in the reoriented domain with the $\langle 001 \rangle /\{001\}$ configuration. (b) The details of the {111} twin boundary and the $\frac{1}{6}\langle 112 \rangle$ Shockley partial dislocation in Fig. 6(a), the misorientation angle $\gamma = 109.5°$. Atoms are colored according to their centrosymmetry values.
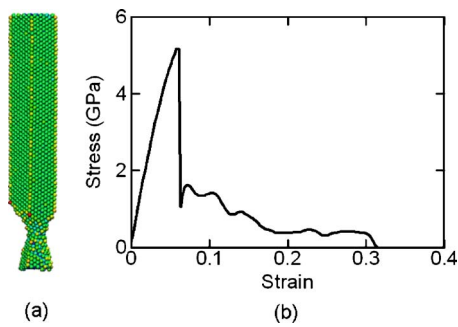
FIG. 6. (Color online) The tensile deformation behavior of an Al wire at 300 K: (a) the deformed configuration at $\varepsilon = 0.13$, and (b) the stress-strain curve. Atoms are colored according to their centrosymmetry values.

gether form hysteretic loops typical of shape memory materials. Since the wires recover their original configurations after unloading, the same behavior is observed in subsequent cycles of loading and unloading, as shown in Fig. 3(b). The minor differences between cycles can be attributed to random thermal oscillations and possible residual defects (discussed later).

B. Irreversible deformation of Al wires

Al wires do not show the pseudoelastic behavior seen for Cu and Ni wires. This difference arises from a different deformation mechanism. Specifically, Al wires first deform elastically during loading. Upon yielding, a necking process starts and quickly leads to thinning and eventual rupture of the wire, as shown in Fig. 6. While twinning is responsible for the lattice reorientation in Cu and Ni wires, slip via full dislocations of the $\frac{1}{2}\langle 110 \rangle$ type is primarily responsible for the necking process in Al wires. The slip mechanism involving full dislocations causes the tensile deformation to be permanent and irreversible upon unloading. Consequently, no pseudoelasticity or SME is possible for such wires.

C. Temperature-dependent transition behavior of Au wires

Au wires show a temperature-dependent transitional behavior between the pseudoelasticity and the plasticity described above. Specifically, at low temperatures, Au wires show similar forward and reverse lattice reorientations through the propagation of twin boundaries as in Cu and Ni wires. However, the reorientation process during loading may not sweep through the entire wire length and necking can occur at the twin boundary before the reorientation process is complete, as shown in Fig. 7(a). The stress plateaus between points A and B for T=5 K and between points C and D for T=50 K in Fig. 7(b) correspond to the lattice orientation from the $\langle 110 \rangle/\{111\}$ configuration to the $\langle 100 \rangle/\{100\}$ configuration. The necking process starts at points B (T=5 K) and D (T=50 K) and leads to the precipitous drop of stresses following these points. If unloading occurs before necking, the Au wires can recover their original $\langle 110 \rangle/\{111\}$ configuration through a reverse lattice reorientation process which is the same as what is seen in Cu and
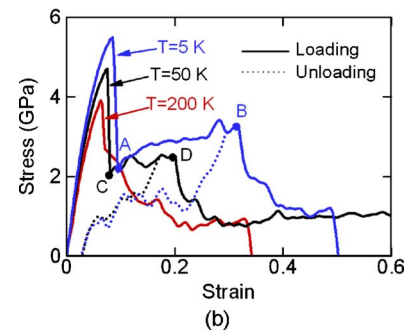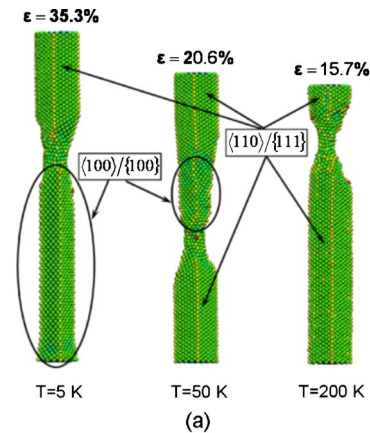
FIG. 7. (Color online) The tensile loading and unloading behavior of Au wires at different temperatures: (a) deformed configurations, and (b) stress-strain curves. Atoms are colored according to their centrosymmetry values.

Ni wires. Once necking occurs, however, the deformation is no longer fully reversible. Consequently, the maximum reversible strains of Au wires are less than those of Cu and Ni wires because of the incomplete reorientation process during loading. The fraction of reoriented lattice ($\langle 100 \rangle/\{100\}$) at the onset of necking decreases as temperature increases, as shown in Fig. 7(a). At T=200 K, no reorientation is observed and necking starts immediately after yielding. This scenario corresponds to the case of Al wires discussed above, with the deformation progressing via slip and being irreversible.

D. Deformation mechanism: Twinning or slip

The different behaviors of Cu, Ni, Au, and Al wires result from different deformation mechanisms. The pseudoelasticity of Cu and Ni is due to the reversible lattice reorientation associated with twin boundary propagation. The irreversible plasticity of Al wires is primarily due to the slip of full dislocations. The mixed occurrence of twinning and slip explains the transitional behavior of Au wires between pseudoelasticity and plasticity. In summary, for the nanowires analyzed twinning leads to pseudoelasticity and slip leads to permanent deformation.

Being two competitive mechanisms in fcc metals, twinning and slip are known to occur under different conditions. Conventional wisdom suggests that metals with low γ_{sf} are more likely to deform through twinning. However, γ_{sf} alone
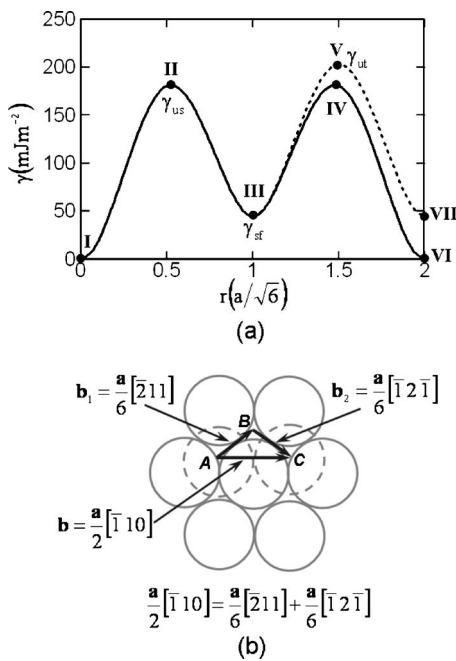
FIG. 8. A schematic illustration of the relationship between a dissociated full location and two partial dislocations.

may not be enough to determine whether a metal would deform via twinning or slip. For example, Ni wires deform via twinning while Al wires deform via slip, even though Ni and Al have similar levels of γ_{sf}. Swygenhoven *et al.* have shown that the competition between twinning and slip is primarily determined by the energy ratio of γ_{sf}/γ_{us}.[26] Specifically, metals with lower γ_{sf}/γ_{us} values are more likely to deform via twinning than slip. This understanding is consistent with the observation that twinning is more likely to occur in Ni wires than in Al wires since $(\gamma_{sf}/\gamma_{us})_{Ni}=0.317$ and $(\gamma_{sf}/\gamma_{us})_{Al}=0.836$. Even though γ_{sf}/γ_{us} provides a better criterion than γ_{sf} for assessing the competition between twinning and slip, it cannot explain all cases and a higher order effect appears to exist. For example, as previously shown, twinning is more likely in Ni wires than in Au wires despite the fact that Ni has a slightly higher ratio of γ_{sf}/γ_{us} (0.317) than Au (0.307). The reason is that the competition is determined by the energy barriers associated with both slip and twinning. While γ_{sf}/γ_{us} only quantifies the energy barrier for slip, the energy barrier for twinning must also be considered.

The competition between twinning and slip can be better explained by the dislocation nucleation criterion of Rice[27] and the twin nucleation criterion of Tadmor and Hai.[9] In Rice's theory, a full $\frac{1}{2}\langle 110\rangle$ type dislocation can be considered as being formed by two $\frac{1}{6}\langle 112\rangle$ type Shockley partial dislocations in two successive steps. This sequence of events is illustrated in Fig. 8. At point I [corresponding to position A of the dashed layer of (111) atoms in Fig. 8(b)], the system is in a stress-free state. The GSFE [vertical axis in Fig. 8(a)] increases as the shear displacement [horizontal axis in Fig. 8(a)] between the two neighboring (111) planes increases. At point II [position B in Fig. 8(b)], the system is at an unstable state and a leading partial dislocation with Burger's vector $\frac{a}{6}[\bar{2}11]$ is formed. In Fig. 5, the emission of this partial is

from the right-hand edge (surface) of the cross section of the nanowire shown. Obviously, the nucleation of this leading partial must overcome the energy barrier γ_{us}. Following the emission, a degree of stress relaxation and energy release occurs, as indicated by the portion of the GSFE curve between points II and III in Fig. 8(a). The stacking fault between the two neighboring (111) planes behind the partial dislocation line corresponds to an elevated energy level of γ_{sf} [point III in Fig. 8(a) and position B in Fig. 8(b)] relative to the perfect fcc stacking sequence at point I in Fig. 8(a) and position A in Fig. 8(b). As loading continues and sufficient energy is imparted to overcome the second energy barrier at the level of γ_{us} [point IV in Fig. 8(a)], a trailing partial dislocation with the Burger's vector $\frac{a}{6}[\bar{1}2\bar{1}]$ is emitted between the same pair of (111) slip planes. The leading and the trailing partials combine to form a full dislocation with the Burger's vector $\frac{a}{2}[\bar{1}10]$. This deformation process can be expressed as

$$\frac{a}{6}[\bar{2}11] + \frac{a}{6}[\bar{1}2\bar{1}] \rightarrow \frac{a}{2}[\bar{1}10]. \tag{1}$$

Obviously, the energy barrier for the nucleation of the trailing partial is $\gamma_{us}-\gamma_{sf}$. The full dislocation represents a permanent unit shift in the fcc stacking sequence and returns the lattice to the original low energy state of point I (or VI). This mechanism is what is responsible for the irreversible deformation in Al wires and Au wires at high temperatures.

Based on Rice's theory, Tadmor and Hai have shown that in the twinning mode, a leading partial is first nucleated from a sharp edge of a surface. Instead of the emission of a trailing partial, a second leading partial (twinning partial) is nucleated on a neighboring slip plane next to the original pair of slip planes. The emission of the twinning partial can be analyzed by the dotted curve in Fig. 8(a). While the solid GSFE curve in Fig. 8(a) characterizes the interplanar energy associated with a slip discontinuity introduced in a perfect crystal; the dotted curve in Fig. 8(a) characterizes the energy to form a microtwin by shearing of a plane adjacent to an existing intrinsic stacking fault formed by the passage of a leading partial. The shearing begins at point III at an elevated energy state (γ_{sf}). A twinning partial is emitted at point V where the energy reaches a maximum of γ_{ut} or the unstable twinning energy. The interplanar energy reaches a new minimum at point VII after the slip of a full Burgers vector. This process allows the twin plane to move one layer in the direction perpendicular to the slip planes. For the nanowires, this process of the nucleation of twinning partials on adjacent layers repeats itself and progressively moves the twin plane along the wire axis, layer by layer. It also results in the reorientation of the $\langle 110\rangle/\{111\}$ wire into the $\langle 100\rangle/\{100\}$ wire.

Clearly, the deformation mode (twinning or full dislocation motion) is determined by the competition between the nucleation of the trailing partial needed to complete the dissociated full dislocation and the nucleation of the twinning partial needed to form a microtwin. Based on the aforementioned dislocation nucleation process, Tadmor and Hai devel-
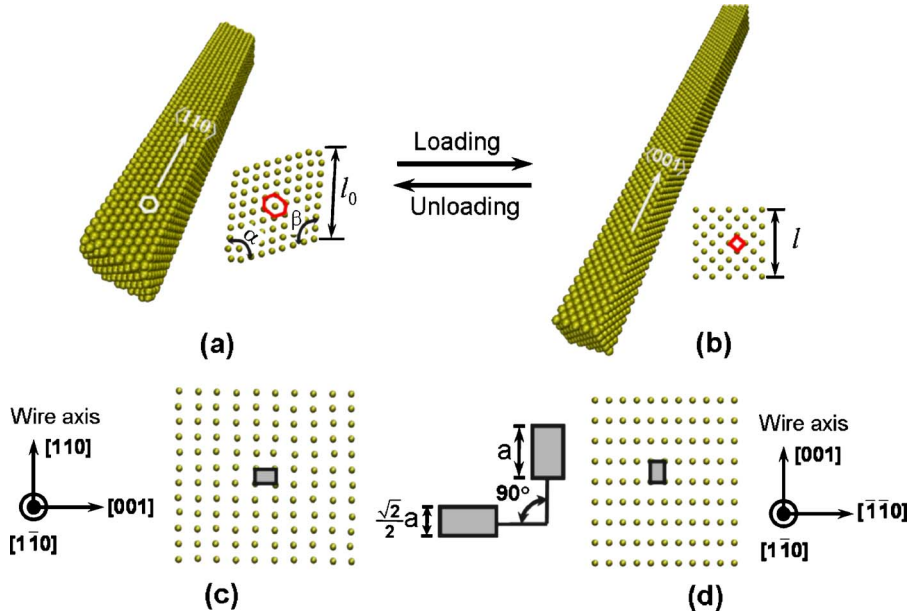
FIG. 9. (Color online) Reversible lattice reorientations upon loading and unloading in single-crystalline metal nanowires; (a) a $\langle 110 \rangle / \{111\}$ Cu wire with rhombic cross sections ($\alpha = 70.5°$ and $\beta = 109.5°$) (b) stretched $\langle 001 \rangle / \{001\}$ wire with square cross sections, (c) $(1\bar{1}0)$ atomic plane containing the [110] wire axis and the long diagonal ([001]) of the rhombic cross section in the original wire, and (d) the same $(1\bar{1}0)$ atomic plane as in (c) after lattice reorientation, containing the new wire axis ([001]) and a diagonal ([$\bar{1}\bar{1}0$]) of the new square cross section.

oped a criterion for the onset of deformation twinning which quantifies the competition between slip and twinning.[9] The related twinnability is

$$\tau_{\mathbf{a}} = \left[1.136 - 0.151 \frac{\gamma_{\mathrm{sf}}}{\gamma_{\mathrm{us}}} \right] \sqrt{\frac{\gamma_{\mathrm{us}}}{\gamma_{\mathrm{ut}}}}. \qquad (2)$$

This parameter depends on both $\gamma_{\mathrm{us}}/\gamma_{\mathrm{ut}}$ and $\gamma_{\mathrm{sf}}/\gamma_{\mathrm{us}}$ which measure the energy barriers associated twinning and slip, respectively. On one hand, twinning is favored when $\gamma_{\mathrm{sf}}/\gamma_{\mathrm{us}}$ is small and $\gamma_{\mathrm{us}}/\gamma_{\mathrm{ut}}$ is large (as in the case of Cu and Ni) because small values of $\gamma_{\mathrm{sf}}/\gamma_{\mathrm{us}}$ indicate higher barriers of $\gamma_{\mathrm{us}} - \gamma_{\mathrm{sf}}$ for the nucleation of the trailing partial and large $\gamma_{\mathrm{us}}/\gamma_{\mathrm{ut}}$ values indicate lower barriers for the nucleation of a twinning partial. On the other hand, slip is favored when $\gamma_{\mathrm{sf}}/\gamma_{\mathrm{us}}$ is large and $\gamma_{\mathrm{us}}/\gamma_{\mathrm{ut}}$ is small (as in the case of Al). As shown in Table I, the twinnability ranking based on interatomic potentials for the metals analyzed is

$$\tau_{\mathbf{a}}^{\mathrm{Cu}} > \tau_{\mathbf{a}}^{\mathrm{Ni}} > \tau_{\mathbf{a}}^{\mathrm{Au}} > \tau_{\mathbf{a}}^{\mathrm{Al}} \qquad (3)$$

This is in good agreement with the results of experiments and first principle calculations. Furthermore, it clearly explains the different behaviors of the fcc nanowires reported here. Cu and Ni exhibit reversible deformations through twinning because it is favored over slip. On the other hand, the deformation of Al wires is irreversible because slip is favored over twinning.

The above analysis does not account for the effect of temperature which is important for Au because it has a twinnability in the transition regime. Our observation of Au wires showing twinning (and therefore, pseudoelasticity and SME) at low temperatures and slip (and therefore, plasticity) at high temperatures is consistent with the experimental observation that twinning tends to occur at lower temperatures.[41,42]

E. Large recoverable strains

The large strains associated with the forward and reverse lattice reorientations can be quantified by a simple crystallographic analysis. The analysis shows that the reversible strains are proportional to the volume fraction of the reoriented lattice, and the maximum strain is 41% for a complete lattice reorientation. Specifically, Figs. 9(c) and 9(d) compares the same $(1\bar{1}0)$ plane in the $\langle 110 \rangle / \{111\}$ [at point A in Fig. 3(a)] and the $\langle 001 \rangle / \{001\}$ configurations [at point C in Fig. 3(a)]. Clearly, the forward (loading) and backward (unloading) lattice reorientations manifest as 90° rotations in opposite directions of the unit cell in the $(1\bar{1}0)$ plane. The length and width of the rectangular unit cell in both cases are, respectively, a and $\frac{\sqrt{2}}{2}a$; where a is the lattice constant in the stressed states and is assumed to be the same at A and C. Hence the axial strain associated with the lattice reorientation between A and C is given by

$$\varepsilon_{\langle 110 \rangle \leftrightarrow \langle 001 \rangle} = \left(a - \frac{\sqrt{2}}{2}a \right) / \frac{\sqrt{2}}{2}a = 0.414. \qquad (4)$$

Obviously, $\varepsilon_{\langle 110 \rangle \leftrightarrow \langle 001 \rangle}$ is an attribute of the fcc structure and is independent of a. Consequently, the pseudoelastic strain associated with the lattice reorientation which constitutes the primary part of the total recoverable strain (ε_r) is the same for wires of all fcc metals and of all sizes. Equation (4) gives the recoverable strain associated with full transformations without residual defects and agrees well with the results of atomistic simulations for Cu and Ni wires. Au wires show smaller $\varepsilon_{\langle 110 \rangle \leftrightarrow \langle 001 \rangle}$ because of the incomplete lattice reorientation. In that case, $\varepsilon_{\langle 110 \rangle \leftrightarrow \langle 001 \rangle}$ is proportional to the volume fraction of the transformed lattice.

In addition to $\varepsilon_{\langle 110 \rangle \leftrightarrow \langle 001 \rangle}$, ε_r also includes the elastic strain $\varepsilon_{\langle 110 \rangle}^e$ associated with the lattice stretching in the $\langle 110 \rangle / \{111\}$ configuration between O and A [Fig. 3(a)] and

the elastic strain $\varepsilon^e_{\langle 001 \rangle}$ associated with the lattice stretching in the $\langle 001 \rangle / \{001\}$ configuration between C and D, i.e.,

$$\varepsilon_r \approx \varepsilon^e_{\langle 110 \rangle} + \varepsilon_{\langle 110 \rangle \leftrightarrow \langle 001 \rangle} + \varepsilon^e_{\langle 001 \rangle} \qquad (5)$$

$\varepsilon^e_{\langle 110 \rangle}$ and $\varepsilon^e_{\langle 001 \rangle}$ are small compared with $\varepsilon_{\langle 110 \rangle \leftrightarrow \langle 001 \rangle}$, and they also vary with material and wire size. As shown in Figs. 3(a) and 4, ε_r are approximately 51% and 45% for Cu and Ni wires, respectively. In particular, for the 1.8×1.8 nm Cu nanowire in Fig. 3, $\varepsilon_r \approx 0.048 + 0.415 + 0.049 = 0.512$. The ε_r for Au wires depends on temperature and is 0.32, 0.20, and 0.07 at 5, 50, and 200 K, respectively.

F. Driving force

The pseudoelastic behavior of SMAs arises from two related but somewhat different mechanisms which yield very similar stress-strain relations like those in Fig. 3. The first mechanism is superelastic and involves a martensitic phase transformation driven by the free energy difference between the parent and product phases. The second mechanism is rubberlike and occurs solely within the martensitic state through reversible movement of twin boundaries.[2,43] This mechanism is driven by a general tendency for the equilibrium symmetry of the short-range order configuration of lattice imperfections to conform to the symmetry of the lattice. Hence aging in the martensitic state and the existence of lattice imperfections are necessary conditions.[44] Clearly, the mechanism responsible for the pseudoelastic behavior of the nanowires analyzed here is more rubberlike than superelastic because the deformation occurs solely within the fcc structure, without any phase change. However, neither aging nor lattice imperfections are involved. Then, what causes the $\langle 001 \rangle / \{001\}$ wire to spontaneously revert back to its original $\langle 110 \rangle / \{111\}$ configuration upon unloading, since both states have the same fcc crystalline structure and, perhaps, the same "stability"? The answer lies in the surfaces and the extremely high surface-to-volume ratios of nanowires which can significantly affect structural stability. Specifically, $\{111\}$ surfaces in fcc metals have the lowest energy among all surfaces. For example, the surface energies of Cu $\{001\}$ and $\{111\}$ planes are 1.35 and 1.24 J m^{-2}, respectively. This difference in surface energy causes the $\langle 110 \rangle / \{111\}$ configuration to have a lower energy and to be more stable compared with the $\langle 001 \rangle / \{001\}$ configuration.

A quantification of the difference in the potential energy as a function of wire size between the two configurations is given in Fig. 10(a) for Cu. Specifically, the quantification is carried out by "slicing" $\langle 001 \rangle / \{001\}$ wires and $\langle 110 \rangle / \{111\}$ wires out of bulk Cu crystals with appropriate orientations and dimensions. The potential energy of the two configurations is computed after they reach their equilibrium states through conjugate gradient energy minimization using molecular statics.[45] The potential energy difference primarily results from the energy density difference between $\{111\}$ and $\{001\}$ surfaces. The average potential energy per atom decreases with increasing wire size for each configuration because smaller wires have larger surface-to-volume ratios. On the other hand, regardless of size, $\langle 110 \rangle / \{111\}$ wires always
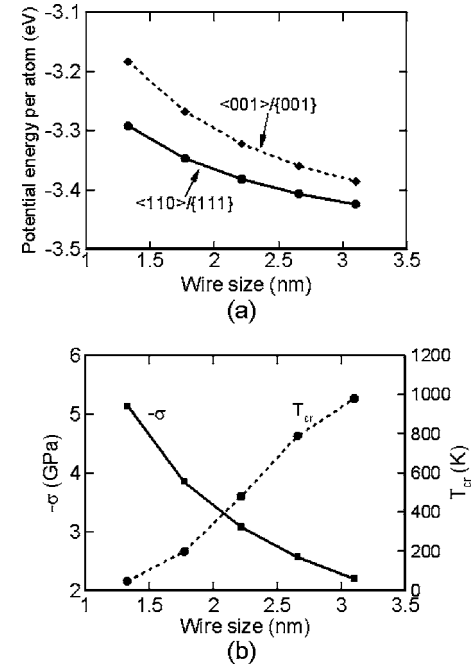
FIG. 10. (a) A comparison of the potential energy per atom of Cu wires with the $\langle 110 \rangle / \{111\}$ and $\langle 001 \rangle / \{001\}$ configurations. (b) Variations of the surface-stress-induced compressive stress σ and the critical temperature T_{cr} with wire size for Cu.

have lower energy levels compared with their deformed counterparts with the $\langle 001 \rangle / \{001\}$ configuration. Therefore the $\langle 001 \rangle / \{001\}$ wire has a natural tendency for spontaneous reorientation back to the $\langle 110 \rangle / \{111\}$ configuration upon unloading. The reorientation essentially lowers the surface energy as a result of the increase in atomic density on surfaces when $\{001\}$ surfaces reorganize into closely packed $\{111\}$ surfaces.

The driving force for the spontaneous reorientation can also be viewed as coming from the surface stress which induces a compressive stress in the interior of the wire. This compressive stress is $\sigma = -4fl/A$, where f is the surface stress of the $\{001\}$ planes in the $\langle 001 \rangle / \{001\}$ configuration, l is the side length of the square cross section [Fig. 9(b)], and $A (=l^2)$ is the corresponding cross-sectional area. Obviously, the magnitude of σ increases as the wire size decreases and can be very high at the nanoscale, as shown in Fig. 10(b). For example, $\sigma = -3.85$ GPa for a $\langle 001 \rangle / \{001\}$ Cu wire with $l = 1.45$ nm ($l_0 = 1.8$ nm in the $\langle 110 \rangle / \{111\}$ state), sufficient for initiating the reverse reorientation at temperatures above 200 K, even in the absence of externally applied forces. Note, however, that σ is only on the order of Pascals in bulk materials and is negligible, providing an explanation as to why a similar behavior is not seen in bulk metals.

IV. SHAPE MEMORY EFFECT

A. Critical temperatures for spontaneous transformation

Like the behavior of normal bulk SMAs, the pseudoelastic behavior of Cu wires reported here is strongly

temperature-dependent. Specifically, the reverse lattice reorientation from $\langle 001 \rangle$ to $\langle 110 \rangle$ occurs only above a size-dependent critical temperature T_{cr} [Fig. 10(b)]. If unloading takes place at temperatures below T_{cr}, the reverse lattice reorientation does not occur and the wire retains the $\langle 001 \rangle / \{001\}$ configuration. When subsequently heated above T_{cr}, the unloaded $\langle 001 \rangle / \{001\}$ wire spontaneously returns to its original $\langle 110 \rangle / \{111\}$ configuration through the reverse lattice reorientation. This is a SME driven by surface stress and the high surface-to-volume ratios of the nanowire. It is a one-way SME that has the $\langle 110 \rangle / \{111\}$ configuration as the parent state. The value of T_{cr} is obtained by gradually heating a $\langle 001 \rangle / \{001\}$ wire until lattice reorientation occurs. The heating starts at 0 K and the temperature is increased by 10 K in each heating step. At each temperature, the wire is relaxed for 150 ps. The reorientation is identified by monitoring the potential energy change during heating. Specifically, the potential energy increases proportionally with temperature if there is no lattice reorientation. However, the potential energy drops precipitously at the occurrence of the lattice reorientation, allowing the onset of the latter to be determined.

If the $\langle 110 \rangle / \{111\}$ state always has a lower energy than the corresponding $\langle 001 \rangle / \{001\}$ state regardless of size, why does the reverse reorientation only occur above T_{cr}? The answer has to do with the energetic barrier and driving force for the process. To initiate the reorientation, partial dislocations nucleate and propagate to accommodate mobile twin boundaries. These defects are of higher energies and thus constitute an energy barrier for the reorientation, which is closely related to unstable stacking fault energy. Thermal energy can provide the necessary energy for overcoming the barrier. As wire size increases, σ decreases and higher temperatures are needed to initiate the spontaneous reverse reorientation, as shown in Fig. 10(b). This size and temperature dependence is frequently observed in experiments. For example, at a given temperature $\langle 001 \rangle / \{001\}$ Au nanowires and nanofilms are observed to reorient into the $\langle 110 \rangle / \{111\}$ state only when their size is reduced to less than 2 nm by electron beam irradiation.[12,37] On the other hand, because of the high energy barrier in Ni, the surface stress induced compressive stress alone cannot initiate the spontaneous lattice reorientation in Ni wires upon unloading even at very high temperatures. Therefore external compressive stress is needed for the reverse lattice reorientation. Similar to the temperature effect in Cu wires, less external compressive stresses are needed as temperature increases in Ni wires.

It is illustrative to point out that the behavior discovered here is likely to be specific to the $\langle 110 \rangle / \{111\}$ and $\langle 001 \rangle / \{100\}$ configurations. Experiments and computations have shown that the axes of most fcc metal nanowires are in the $\langle 001 \rangle$, $\langle 110 \rangle$, or $\langle 111 \rangle$ orientations.[18] The first two orientations are involved in the reorientation processes discussed in this paper. The third orientation involves nanowires with $\langle 111 \rangle$ axes and $\{111\}$ cross sections. Calculations carried out in this work show that such wires do not exhibit the

pseudoelasticity and SME the $\langle 110 \rangle / \{111\}$ and $\langle 001 \rangle / \{100\}$ wires show. This is perhaps partly because the $\langle 111 \rangle$ axes and $\{111\}$ cross sections of these wires give rise to smaller resolved shear stresses (rss) on the $\frac{a}{6}\{111\}\langle 11\bar{2} \rangle$ slip systems which are a driving force for the partial dislocation nucleation and lattice reorientations responsible for the SME observed here.

The T_{cr} and wire size for relaxation are closely related to the $\{111\}$ and $\{001\}$ surface energies, surface stresses, and unstable stacking fault energy of each metal. Therefore the size-dependent T_{cr} varies from material to material. For example, Cu wires with lateral dimensions between 1.3 and 3.1 nm exhibit SME with T_{cr} ranges from 50 to 1000 K. However, T_{cr} for Ni wires of the same size range are so high that it approaches a significant fraction of the melting point. Under such conditions, the SME is no longer obvious because the wire behavior becomes disorganized and dominated by random thermal vibrations. On the other hand, Ni wires with defects can exhibit SME because T_{cr} can be lowered by surface and internal structural defects such as vacancies, kinks, and local lattice distortions. Specifically, the presence of defects lowers the T_{cr} and essentially shifts the SME toward larger wires because higher energies associated with disorders facilitate the initiation of twin boundaries. These defects may result from manufacturing processes and can also be nucleated and annihilated during cyclic loading and unloading. Defects may also affect the stress-strain responses and reduce ε_r by causing incomplete reorientation, as discussed earlier. However, this effect may be relatively small as shown in Fig. 3(b) if the initial state of the wires is nearly defect-free. In summary, the material and size dependence of T_{cr} suggest a class of nano building blocks with an SME useful over a wide range of temperature.

B. Effect of size on SME

fcc metals in bulk have not been known to possess shape memory. One logical question is why fcc nanowires exhibit shape memory and pseudoelasticity but their bulk counterparts do not. The reason lies in their extremely small sizes at the nanometer scale and their unique one-dimensional (1D) structure. First of all, it has been demonstrated that twinning is vital to the pseudoelasticity in the nanowires. Slip is generally favored over twinning in bulk fcc metals under normal loading conditions. Twinning becomes a viable deformation mode only when the dominant size (e.g., grain size or wire size) scale approaches nanometers. Specifically, both experiments and simulations have shown that twinning is the primary deformation mechanism in nanocrystalline metals, nanowires, and nanoparticles.[36] Second, nanowires have extremely large surface-to-volume ratios. Specifically, a nanowire has a surface-to-volume ratio 10^6 times that of a macroscopic specimen.[19] The fraction of surface atoms is around 39.5% for a 1.8×1.8 nm nanowire while that for bulk metals approaches zero. As previously discussed, the high surface-to-volume ratios induce high values of internal compressive stress σ which are on the order of GPa, providing the
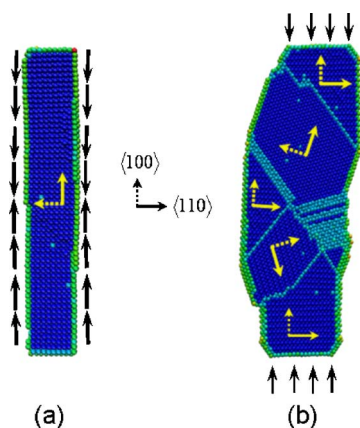
FIG. 11. (Color online) Size effect on the shape memory of metal nanowires: (a) a 1.45×1.45 nm Cu wire fully reoriented under surface stress, and (b) a 3.6×3.6 nm $\langle 100 \rangle / \{100\}$ Cu wire partially reoriented under external compression, the yellow coordinate axes indicate the different orientations of the grains separated by twin boundaries. Atoms are colored according to their centrosymmetry values.

necessary driving force for the reverse reorientation above T_{cr}, even in the absence of externally applied forces, as shown in Fig. 11(a). On the other hand, σ is only on the order of pascals in bulk materials, far from being sufficient to initiate spontaneous lattice reorientations. One may still wonder if a bulk fcc crystal with the $\langle 110 \rangle / \{111\}$ configuration would exhibit the lattice reorientation leading to pseudoelasticity and shape memory in nanowires under the condition that an external compressive stress of sufficient magnitude is applied. The answer is clearly "no" because the reversibility of the reorientation process primarily results from the unique 1D structure at the nanoscale. This structure acts as a channel, limiting the propagation of twin boundaries to the direction of the wire axis. The opposite directions of twin boundary propagation during loading and unloading give rise to the reversible nature of deformations, as shown in Fig. 11(a). As the lateral dimensions increase, the wire gradually becomes a 3D structure with multiple modes of defect nucleation, propagation and interaction. Such a 3D structure leads to simultaneous twin boundaries and stacking faults at multiple sites and in multiple directions,[35] as shown in Fig. 11(b). The entanglement and interactions of these defects reduce the mobility of the twin boundaries and ultimately preclude the occurrence of the pseudoelasticity and the shape memory. Under such conditions, the wires are essentially a polycrystal with grains separated by interlocking twin boundaries.

V. SUMMARY AND CONCLUSIONS

(1) The mechanical behavior of Cu, Ni, Au, and Al nanowires with lateral dimensions between 1 and 5 nm and $\langle 110 \rangle / \{111\}$ configurations are analyzed using MD simulations. Upon tensile loading and unloading, Cu and Ni wires exhibit a pseudoelastic behavior with large reversible strains of up to 50%, well beyond the recoverable strains of 5%–8%

typical for most bulk shape memory alloys (SMAs). In comparison, the tensile deformations of Al wires are irreversible upon unloading. Au wires show a transition of behavior from pseudoelasticity at low temperatures to plasticity at high temperatures and have temperature-dependent reversible strains which decrease with temperature.

(2) The difference in behavior among wires of different materials is due to two competing deformation mechanisms, i.e., twinning and slip. Specifically, the pseudoelasticity of Cu and Ni wires exists only at the nanometer scale and is associated with a reversible crystallographic lattice reorientation through twin boundary propagation. On the other hand, the irreversible tensile deformation of Al wires is due to crystalline slip. The transitional behavior of Au wires is due to a change in deformation mechanism from twinning at low temperatures to slip at high temperatures. The competition between twinning and slip is important in understanding the pseudoelastic behavior and the SME of the fcc nanowires. fcc metals with high twinnability (such as Cu, Ni, and Au) favor twinning which leads to the pseudoelastic behavior and SME in their nanowires. On the other hand, fcc metals with low twinnability (such as Al) favor slip which leads to irreversible deformations even at the nanoscale.

(3) A temperature-dependent spontaneous lattice reorientation enables wires in the $\langle 100 \rangle / \{100\}$ configuration to revert to the $\langle 110 \rangle / \{111\}$ configuration through heating. This temperature effect leads to an SME in Cu wires and in Au wires at lower temperatures. Specifically, the $\langle 110 \rangle / \{111\}$ configuration is more stable than the $\langle 100 \rangle / \{100\}$ configuration primarily because $\{111\}$ surfaces have a lower surface energy than that of $\{100\}$ surfaces. Driven by the high surface-stress-induced internal stresses at the nanoscale, $\{100\}$ surfaces spontaneously reconstruct into lower energy $\{111\}$ surfaces as part of the lattice reorientation process to lower the overall free energy. This spontaneous process only occurs at temperatures above a critical value T_{cr} which is material specific. This is because sufficient thermal energy is required to overcome the energy barrier for initiating the process. For each material, T_{cr} increases with wire size because the driving force is smaller in larger wires and hence a higher amount of thermal energy is needed.

(4) The unique pseudoelasticity and SME only exist in nanowires of fcc metals with high twinnability, but not in their bulk form. This size effect is primarily due to three reasons: (i) the small size scales in fcc metals make twinning the favored deformation mechanism, (ii) the surface-stress-induced internal compressive stress in nanowires is on the order of GPa because of their high surface-to-volume ratios and this internal compressive stress provides the necessary driving force for a spontaneous lattice reorientation without external influence, and (iii) the reversibility of the lattice reorientation process is derived from the unique 1D structure of the nanowires. As their lateral dimensions increase, nanowires become 3D structures. Under such conditions, the interaction and entanglement of twin planes transform the wires into polycrystals and ultimately preclude the occurrence of the lattice reorientation which is the mechanism for the pseudoelasticity at the nanoscale.

*Corresponding author. FAX: 404-894-0186. Email address: min.zhou@gatech.edu

[1] K. Otsuka and X. Ren, Intermetallics **7**, 511 (1999).

[2] K. Otsuka and C. M. Wayman (Cambridge University Press, New York, 1998), p. 282.

[3] U. Landman, W. D. Luedtke, B. E. Salisbury, and R. L. Whetten, Phys. Rev. Lett. **77**, 1362 (1996).

[4] B. I. Yakobson, C. J. Brabec, and J. Bernholc, Phys. Rev. Lett. **76**, 2511 (1996).

[5] M. R. Falvo, G. J. Clary, R. M. T., II, V. Chi, F. P. B., Jr., S. Washburn, and R. Superfine, Nature (London) **389**, 582 (1997).

[6] W. Liang and M. Zhou, Nano Lett. **5**, 2039 (2005).

[7] S. Büttgenbach, S. Bütefish, M. Leester-Schädel *et al.*, Microsyst. Technol. **7**, 165 (2001).

[8] F. Patolsky and C. M. Lieber, Mater. Today **8**, 20 (2005).

[9] E. B. Tadmor and S. Hai, J. Mech. Phys. Solids **51**, 765 (2003).

[10] H. S. Park and J. A. Zimmerman, Scr. Mater. **54**, 1127 (2006).

[11] J. C. González, V. Rodrigues, J. Bettini, L. G. C. Rego, A. R. Rocha, P. Z. Coura, S. O. Santas, F. Sato, D. S. Galvao, and D. Ugarte, Phys. Rev. Lett. **93**, 126103 (2004).

[12] Y. Kondo and K. Takayanagi, Phys. Rev. Lett. **79**, 3455 (1997).

[13] Z. Liu, Y. Yang, J. Liang, Z. Hu, S. Li, S. Peng, and Y. Qian, J. Phys. Chem. B **107**, 12658 (2003).

[14] J. Diao, K. Gall, and M. L. Dunn, Phys. Rev. B **70**, 075413 (2004).

[15] L. G. C. Rego, A. R. Rocha, V. Rodrigues, and D. Ugarte, Phys. Rev. B **67**, 045412 (2003).

[16] V. Rodrigues, J. Bettini, A. R. Rocha, L. G. C. Rego, and D. Ugarte, Phys. Rev. B **65**, 153402 (2002).

[17] V. Rodrigues and D. Ugarte, Nanotechnology **13**, 404 (2002).

[18] V. Rodrigues and D. Ugarte, in *Nanowires and Nanobelts: Materials, Properties and Devices*, edited by Z. L. Wang (Springer, New York, 2003), p. 177.

[19] W. Liang and M. Zhou, J. Eng. Mater. Technol. **127**, 423 (2005).

[20] Y. Oshima, H. Koizumi, K. Mouri, H. Hirayama, K. Takayanagi, and Y. Kondo, Phys. Rev. B **65**, 121401(R) (2002).

[21] K. Gall, J. Diao, and M. L. Dunn, Nano Lett. **4**, 2431 (2004).

[22] Y. Mishin, D. Farkas, M. J. Mehl, and D. A. Papaconstantopoulos, Phys. Rev. B **59**, 3393 (1999).

[23] Y. Mishin, M. J. Mehl, D. A. Papaconstantopoulos, A. F. Viter, and J. D. Kress, Phys. Rev. B **63**, 224106 (2001).

[24] H. S. Park and J. A. Zimmerman, Phys. Rev. B **72**, 054106 (2005).

[25] J. A. Zimmerman, H. Gao, and F. F. Abraham, Modell. Simul. Mater. Sci. Eng. **8**, 103 (2000).

[26] H. V. Swygenhoven, P. M. Derlet, and A. G. Frøseth, Nat. Mater. **3**, 399 (2004).

[27] J. R. Rice, J. Mech. Phys. Solids **40**, 239 (1992).

[28] E. B. Tadmor and N. Bernstein, J. Mech. Phys. Solids **52**, 2507 (2004).

[29] C. B. Carter and I. L. F. Ray, Philos. Mag. **35**, 189 (1977).

[30] R. W. Balluffi, J. Nucl. Mater. **69&70**, 240 (1978).

[31] W. M. Stobbs and C. H. Sworn, Philos. Mag. **24**, 1365 (1971).

[32] L. E. Murr, *Interfacial Phenomena in Metals and Alloys* (Addison-Wesley, Reading, MA, 1975).

[33] R. H. Rautioaho, Phys. Status Solidi B **112**, 83 (1982).

[34] K. H. Westmacott and R. L. Peck, Philos. Mag. **23**, 611 (1971).

[35] W. Liang and M. Zhou, J. Mech. Eng. Sci. **218**, 599 (2004).

[36] D. P. Field, B. W. True, T. M. Lillo, and J. E. Flinn, Mater. Sci. Eng., A **372**, 173 (2004).

[37] Y. Kondo, Q. Ru, and K. Takayanagi, Phys. Rev. Lett. **82**, 751 (1999).

[38] J. Diao, K. Gall, and M. Dunn, Nat. Mater. **2**, 656 (2003).

[39] A. Hasmy and E. Medina, Phys. Rev. Lett. **88**, 096103 (2002).

[40] H. Ohnishi, Y. Kondo, and K. Takayanagi, Nature (London) **395**, 780 (1998).

[41] R. W. Hertzberg, *Deformation and Fracture Mechanics of Engineering Materials* (Wiley, New York, 1989).

[42] C. Meyers, *Mechanical Metallurgy Principle and Applications* (Prentice-Hall, Englewood Cliffs, NJ, 1984).

[43] R. W. Cahn, Nature (London) **374**, 120 (1995).

[44] X. Ren and K. Otsuka, Nature (London) **389**, 579 (1997).

[45] M. C. Payne, M. P. Teter, D. C. Allan, T. A. Arias, and J. D. Joannopoulos, Rev. Mod. Phys. **64**, 1045 (1992).

[46] S. J. Plimpton, J. Comput. Phys. **117**, 1 (1995).